Causal Approximate Inversion for Control of Structurally Flexible Manipulators Using Nonlinear Inner–Outer Factorization

A. G. Cree
University of Canterbury
Department of Mechanical Engineering
Private Bag 4800
Christchurch, New Zealand

C. J. Damaren*
University of Toronto
Institute for Aerospace Studies
4925 Dufferin Street
Toronto, ON M3H 5T6 Canada
e-mail: damaren@utias.utoronto.ca

Received 20 November 2000; accepted 3 January 2001

A control scheme for flexible-link manipulators is advanced which is based on the notion of nonlinear inner–outer factorization. It is well known that the inverse of the forward dynamics map from joint torques to manipulator tip motion is noncausal and cannot be implemented in conjunction with real-time path planning. The methods used here determine causal approximations for the inverse dynamics using the inverse of the outer (stable and minimum phase) factor and a static approximation for the inverse of the inner (lossless but nonminimum phase) factor. The Hamilton–Jacobi equation that arises is approximated by a state-dependent Riccati equation at each time step. The factorization procedure yields the corresponding joint trajectories which can serve as reference trajectories for closing joint-based feedback loops. Experimental results from a planar three-link manipulator with two flexible links demonstrate the efficacy of the procedure.

* To whom all correspondence should be addressed.

1. INTRODUCTION

Typical tracking controllers for controlling the motion of mechanical systems exhibit a combined feedforward–feedback structure. When the plant input and output are collocated, as in the case of joint-based control of rigid robots, perfect inversion can be accomplished with a causal feedforward that corresponds to the inverse dynamics. Feedback stabilization of the error dynamics can be accomplished using feedback linearization or passivity-based techniques. For structurally flexible systems exhibiting collocation, inversion can be accomplished at the joint level[1] but the problem of determining suitable joint trajectories for prescribed endpoint motion remains.

In the noncollocated case, the dynamics are typically nonminimum phase. Hence, feedforward design via plant inversion as well as the corresponding feedback design problem are complicated. In the multi-input/multi-output (MIMO) case, the problem is also nonlinear. Exact inversion strategies have been presented by a number of authors. Noncausal inverses for flexible manipulators have been presented using Fourier techniques.[2] Generalizations of the method have been presented by Devasia et al.[3] and implemented on flexible robots.[4] A time-domain methodology exploiting the two-sided Laplace transform was used by Kwon and Book[5] in the single-link case.

In the present work, we are interested in the case where the feedforward is restricted to be causal necessitating the use of an approximate inverse of the input–output dynamics. Paden et al.[6] have shown that good endpoint tracking can be achieved by delaying the noncausal feedforward of Bayo et al.[2] in conjunction with passive joint-based feedback. Other authors have modified the output of the system so as to achieve minimum phase or passive behavior.[7–9]

In the linear SISO case, transform techniques have been heavily exploited. Gross and Tomizuka[10] and Torfs et al.[11] have used variations of Tomizuka's zero-phase error tracking (ZPET) scheme in discrete time. This class of methodologies approximate the unstable zeros of the plant (which become unstable poles in the inverse) so as to preserve the phase characteristics of the inverse but magnitude errors are incurred. Unfortunately the ZPET technique has not been extended to the MIMO case or to nonlinear systems.

Another approach to approximating the inverse of a transfer function relies on the notion of inner–outer (all-pass/minimum phase) factorizations. The outer portion of the factorization represents the invertible portion of the system while the all-pass inner factor has unity gain and carries the unstable zeros. Its approximation is the key issue. Writing a square transfer matrix as $\mathbf{G}(s) = \Theta(s)\mathbf{R}(s)$ with $\mathbf{R}(s)$ outer and $\Theta(s)$ inner, Shaked[12] has shown that a feedforward signal generated by $\mathbf{R}^{-1}(s)\Theta^{-1}(0)$ generates optimal step responses in L_2 norm. This inversion scheme preserves the magnitude characteristics (singular values) of the inverse and is readily applicable to the MIMO case.

Recently, inner–outer factorizations for certain classes of nonlinear systems have been advanced by Ball and van der Schaft.[13] This allows approximate causal inverses to be constructed along the lines of the linear case. Furthermore, state trajectories of this inverse are the same as those of the plant when it is forced by the feedforward signal from the inverse. This permits trajectory planning for the collocated joint variables which can be input into a robust feedback scheme such as a PD controller.

The bottleneck in generating such approximations is the solution of a Hamilton–Jacobi equation which is the nonlinear analog of the Riccati equation encountered in the linear case. An approximate solution is obtained here using a state-dependent Riccati equation which results from writing the dynamics in an apparent linear form with state-dependent coefficient matrices. Experimental results are presented for a three-link flexible manipulator operating in the plane. Good trajectory tracking is demonstrated using a feedforward based on the inverse of the outer factor and a static (DC) approximation to the inverse of the inner factor coupled with a joint-based feedback.

2. NONLINEAR INNER–OUTER FACTORIZATION

Consider a square nonlinear state–space model of the following form

$$\mathcal{G}: \begin{cases} \dot{\mathbf{x}} = \mathbf{a}(\mathbf{x}) + \mathbf{b}(\mathbf{x})\mathbf{u} \\ \mathbf{y} = \mathbf{c}(\mathbf{x}) + \mathbf{d}(\mathbf{x})\mathbf{u} \end{cases} \tag{1}$$

It is assumed that the model is controllable, observable, and asymptotically stable with $\mathbf{d}(\mathbf{x})$ invertible. The inverse system is given by

$$\mathcal{G}^{-1}: \begin{cases} \dot{\mathbf{x}} = \mathbf{a}(\mathbf{x}) - \mathbf{b}(\mathbf{x})\mathbf{d}^{-1}(\mathbf{x})\mathbf{c}(\mathbf{x}) \\ \qquad\quad + \mathbf{b}(\mathbf{x})\mathbf{d}^{-1}(\mathbf{x})\mathbf{y} \\ \mathbf{u} = -\mathbf{d}^{-1}(\mathbf{x})\mathbf{c}(\mathbf{x}) + \mathbf{d}^{-1}(\mathbf{x})\mathbf{y} \end{cases} \tag{2}$$

To fix ideas, begin with the linear time-invariant case where $\mathbf{a}(x) = \mathbf{A}\mathbf{x}$, $\mathbf{b}(x) = \mathbf{B}$, $\mathbf{c}(x) = \mathbf{C}\mathbf{x}$, and $\mathbf{d}(x) = \mathbf{D}$ with corresponding transfer matrix

$$\mathbf{G}(s) = \left[\begin{array}{c|c} \mathbf{A} & \mathbf{B} \\ \hline \mathbf{C} & \mathbf{D} \end{array}\right] \triangleq \mathbf{C}(s\mathbf{1} - \mathbf{A})^{-1}\mathbf{B} + \mathbf{D}$$

Recall that if $\mathbf{G}^{-1}(s)$ is stable, then $\mathbf{G}(s)$ is minimum phase. If $\mathbf{G}(s)$ is stable and minimum phase, then it is outer. A stable transfer matrix $\Theta(s)$ that is all-pass (inner) satisfies $\Theta^H(j\omega)\Theta(j\omega) = \mathbf{1}\ \forall \omega \in R$. It is a well-known fact[14] that a stable $\mathbf{G}(s)$ with $\mathbf{G}^H(j\omega)\mathbf{G}(j\omega) > \mathbf{O}$, $\omega \in [0, \infty]$, admits an inner–outer factorization $\mathbf{G}(s) = \Theta(s)\mathbf{R}(s)$. In fact,

$$\left[\begin{array}{c} \mathbf{R}^{-1}(s) \\ \Theta(s) \end{array}\right] = \left[\begin{array}{c|c} \mathbf{A} + \mathbf{B}\mathbf{F} & \mathbf{B}\mathbf{D}^{-1} \\ \hline \mathbf{F} & \mathbf{D}^{-1} \\ \mathbf{C} + \mathbf{D}\mathbf{F} & \mathbf{1} \end{array}\right] \tag{3}$$

where $\mathbf{F} = -(\mathbf{D}^{\mathrm{T}}\mathbf{D})^{-1}(\mathbf{B}^{\mathrm{T}}\mathbf{X} + \mathbf{D}^{\mathrm{T}}\mathbf{C})$ and $\mathbf{X} \geq \mathbf{O}$ is the stabilizing solution of the algebraic Riccati equation

$$\begin{aligned} &\mathbf{X}(\mathbf{A} - \mathbf{B}\mathbf{D}^{-1}\mathbf{C}) + (\mathbf{A} - \mathbf{B}\mathbf{D}^{-1}\mathbf{C})^{\mathrm{T}}\mathbf{X} \\ &\quad - \mathbf{X}\mathbf{B}(\mathbf{D}^{\mathrm{T}}\mathbf{D})^{-1}\mathbf{B}^{\mathrm{T}}\mathbf{X} = \mathbf{O} \end{aligned} \tag{4}$$

Now, let $\mathbf{y}_d(t)$ be the desired output of $\mathbf{G}$. In the minimum phase case, the corresponding input is $\mathbf{u}_d(s) = \mathbf{G}^{-1}(s)\mathbf{y}_d(s)$. If one admits the possibility of a noncausal feedforward compensation scheme, then the indicated inverse can be implemented using the two-sided inverse Laplace transform where poles of $\mathbf{G}^{-1}(s)$ in $Re\{s\} > 0$ give rise to $\mathbf{u}_d(t)$, $t < 0$. If a causal feedforward is desired then, $\mathbf{G}^{-1}(s)$ must be approximated. Let $\mathbf{u}(s) = \mathbf{H}(s)\mathbf{y}_d(s)$ denote the feedforward compensation. Then, $\mathbf{y} - \mathbf{y}_d = [\mathbf{1} - \mathbf{G}(s)\mathbf{H}(s)]\mathbf{y}_d$. If $\mathbf{y}_d(t) = \mathbf{r}H(t)$, a step input, then Shaked[12] has noted that $||\mathbf{y} - \mathbf{y}_d||_2$ is minimized by using $\mathbf{H}(s) = \mathbf{R}^{-1}(s)\Theta^{-1}(0)$, which gives in general, $\mathbf{y}(s) = \Theta(s)\Theta^{\mathrm{T}}(0)\mathbf{y}_d(s)$. Therefore, $||\mathbf{y}||_2 = ||\mathbf{y}_d||_2$.

Since this approximation preserves the DC gain of the inverse, the steady-state properties are similar. Let $\boldsymbol{\xi}_d(t)$ be such that $d^n\boldsymbol{\xi}_d/dt^n = \mathbf{y}_d(t)$ with $\boldsymbol{\xi}_d(0) = \cdots = \boldsymbol{\xi}_d^{(n-1)}(0) = \mathbf{0}$ and assume that $\lim_{t\to\infty} \boldsymbol{\xi}_d(t) = \bar{\boldsymbol{\xi}}_d$ exists. Define $\boldsymbol{\xi}$ similarly using $\mathbf{y}(t)$. Using a simple Laplace transform argument, $\bar{\boldsymbol{\xi}} = \bar{\boldsymbol{\xi}}_d$ given the preservation of the DC gain. This is particularly important in motion control applications where $\mathbf{y}$ will typically be acceleration and we desire steady-state position regulation.

In the nonlinear case, a system $\mathcal{G}$ is outer if $\mathcal{G}$ and $\mathcal{G}^{-1}$ are stable. We say that $\mathcal{G}$ is lossless if there exists a storage function $V(\mathbf{x}) \geq 0$ with $V(\mathbf{0}) = 0$ such that

$$V[\mathbf{x}(t_1)] - V[\mathbf{x}(t_0)] = \frac{1}{2}\int_{t_0}^{t_1} \left(\mathbf{u}^{\mathrm{T}}\mathbf{u} - \mathbf{y}^{\mathrm{T}}\mathbf{y}\right) dt \tag{5}$$

Taking $\mathbf{x}(t_0) = \mathbf{0}$ and letting $t_1 \to \infty$ shows that these systems have unity L_2-gain.

Now consider the nonlinear system in (1). An inner–outer factorization will be of the form $\mathcal{G} = \Theta \circ \mathcal{R}$ where $\mathcal{R}$ is outer and Θ is lossless. According to Ball and van der Schaft,[13] one possible factorization is given by

$$\mathcal{R}^{-1}: \begin{cases} \dot{\tilde{\mathbf{x}}} = \mathbf{a}(\tilde{\mathbf{x}}) - \mathbf{b}(\tilde{\mathbf{x}})\mathbf{d}^{-1}(\tilde{\mathbf{x}})\bar{\mathbf{c}}(\tilde{\mathbf{x}}) \\ \qquad\quad + \mathbf{b}(\tilde{\mathbf{x}})\mathbf{d}^{-1}(\tilde{\mathbf{x}})\bar{\mathbf{y}}_d \\ \bar{\mathbf{u}}_d = -\mathbf{d}^{-1}(\tilde{\mathbf{x}})\bar{\mathbf{c}}(\tilde{\mathbf{x}}) + \mathbf{d}^{-1}(\tilde{\mathbf{x}})\bar{\mathbf{y}}_d \end{cases} \tag{6}$$

The inner factor is $\Theta = \mathcal{G} \circ \mathcal{R}^{-1}$ and satisfies

$$\Theta: \begin{cases} \dot{\mathbf{x}} = \mathbf{a}(\mathbf{x}) - \mathbf{b}(\mathbf{x})\mathbf{d}^{-1}(\mathbf{x})\bar{\mathbf{c}}(\mathbf{x}) \\ \qquad\quad + \mathbf{b}(\mathbf{x})\mathbf{d}^{-1}(\mathbf{x})\bar{\mathbf{y}}_d \\ \mathbf{y} = \mathbf{c}(\mathbf{x}) - \bar{\mathbf{c}}(\mathbf{x}) + \bar{\mathbf{y}}_d \end{cases} \tag{7}$$

where

$$\bar{\mathbf{c}}(\mathbf{x}) = \mathbf{c}(\mathbf{x}) + \mathbf{d}^{-1}(\mathbf{x})\mathbf{b}^{\mathrm{T}}(\mathbf{x})P_{\mathbf{x}}^{\mathrm{T}}(\mathbf{x}) \tag{8}$$

Here $P_{\mathbf{x}}(\mathbf{x}) = \partial P/\partial \mathbf{x}^{\mathrm{T}}$ and $P(\mathbf{x})$ satisfies the Hamilton–Jacobi equation

$$\begin{aligned} &P_{\mathbf{x}}(\mathbf{x})[\mathbf{a}(\mathbf{x}) - \mathbf{b}(\mathbf{x})\mathbf{d}^{-1}(\mathbf{x})\mathbf{c}(\mathbf{x})] \\ &\quad - \frac{1}{2}P_{\mathbf{x}}(\mathbf{x})\mathbf{b}(\mathbf{x})[\mathbf{d}^{\mathrm{T}}(\mathbf{x})\mathbf{d}(\mathbf{x})]^{-1}\mathbf{b}^{\mathrm{T}}(\mathbf{x})P_{\mathbf{x}}^{\mathrm{T}}(\mathbf{x}) = \mathbf{O} \end{aligned} \tag{9}$$

subject to the constraint that

$$\begin{aligned} \dot{\mathbf{x}} &= \mathbf{a}(\mathbf{x}) - \mathbf{b}(\mathbf{x})\mathbf{d}^{-1}(\mathbf{x})\mathbf{c}(\mathbf{x}) \\ &\quad - \mathbf{b}(\mathbf{x})[\mathbf{d}^{\mathrm{T}}(\mathbf{x})\mathbf{d}(\mathbf{x})]^{-1}\mathbf{b}^{\mathrm{T}}(\mathbf{x})P_{\mathbf{x}}^{\mathrm{T}}(\mathbf{x}) \end{aligned} \tag{10}$$

is Lyapunov stable. If the state vectors of $\Theta = \mathcal{G} \circ \mathcal{R}^{-1}$ and $\mathcal{R}^{-1}$ satisfy $\mathbf{x}(0) = \tilde{\mathbf{x}}(0)$, then $\mathbf{x}(t) = \tilde{\mathbf{x}}(t)$ for all $t > 0$. Hence, the state of $\mathcal{R}^{-1}$ evolves in an identical manner to that of $\mathcal{G}$ when $\mathcal{G}$ is forced by the output of $\mathcal{R}^{-1}$. This permits the use of the state vector of $\mathcal{R}^{-1}$ as a reference trajectory for feedback design involving $\mathcal{G}$. In the sequel, we drop the $\bar{(\cdot)}$ in (6).

The inverse of $\mathcal{G}$ can be taken as $\mathcal{G}^{-1} = \mathcal{R}^{-1} \circ \Theta^{-1}$ but unless $\mathcal{G}$ is minimum phase, Θ^{-1} will be unstable. Analogous to the linear case, we approximate Θ^{-1} by its static counterpart Θ_{ss}^{-1}. This is obtained by

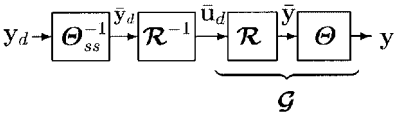

Figure 1. The system $\mathcal{G}$ and its causal inverse.

applying the inverse pattern in (2)–(7) followed by setting $\dot{\mathbf{x}} = \mathbf{0}$

$$\Theta_{ss}^{-1}: \begin{cases} \mathbf{a}(\mathbf{x}) - \mathbf{b}(\mathbf{x})\mathbf{d}^{-1}(\mathbf{x})\mathbf{c}(\mathbf{x}) \\ \quad = -\mathbf{b}(\mathbf{x})\mathbf{d}^{-1}(\mathbf{x})\mathbf{y}_d \\ \bar{\mathbf{y}}_d = \bar{\mathbf{c}}(\mathbf{x}) - \mathbf{c}(\mathbf{x}) + \mathbf{y}_d \end{cases} \tag{11}$$

The system $\mathcal{G}$ and its causal (approximate) inverse are illustrated in Figure 1.

3. DYNAMIC MODELING

The dynamics of a flexible manipulator are assumed to be governed by motion equations of the form

$$M(\mathbf{q})\ddot{\mathbf{q}} + [\widehat{D} + \widehat{C}(\mathbf{q}, \dot{\mathbf{q}})]\dot{\mathbf{q}} + K\mathbf{q} = \widehat{B}\mathbf{u} \tag{12}$$

where $\mathbf{q} = \text{col}\{\boldsymbol{\theta}, \mathbf{q}_e\}$ with $\boldsymbol{\theta}$ denoting the joint angles and $\mathbf{q}_e$ are the elastic coordinates. The joint torques are denoted by $\mathbf{u}$ and the various matrices can be partitioned as

$$M = \begin{bmatrix} M_{\theta\theta} & M_{\theta e} \\ M_{\theta e}^{\mathrm{T}} & M_{ee} \end{bmatrix} \quad \widehat{D} = \begin{bmatrix} \widehat{D}_{\theta\theta} & \mathbf{O} \\ \mathbf{O} & \widehat{D}_{ee} \end{bmatrix} \tag{13}$$

$$K = \begin{bmatrix} \mathbf{O} & \mathbf{O} \\ \mathbf{O} & K_{ee} \end{bmatrix} \quad \widehat{B} = \begin{bmatrix} \mathbf{1} \\ \mathbf{O} \end{bmatrix} \tag{14}$$

Here, M is the mass matrix, K is the stiffness matrix, $\widehat{D}$ is the damping matrix which models structural damping and viscous joint damping, and $\widehat{C}\dot{\mathbf{q}}$ are the nonlinear rate effects.

The tip motion is described by the forward kinematical map $\boldsymbol{\rho} = \mathcal{F}(\mathbf{q})$ and the tip rates can be written in terms of the Jacobian matrix as $\dot{\boldsymbol{\rho}} = J\dot{\mathbf{q}}$ where $J = [J_\theta \; J_e]$. The tip acceleration satisfies

$$\begin{aligned} \ddot{\boldsymbol{\rho}} = J\ddot{\mathbf{q}} + \dot{J}\dot{\mathbf{q}} = -JM^{-1}(\widehat{D} + \widehat{C})\dot{\mathbf{q}} - JM^{-1}K\mathbf{q} \\ + JM^{-1}\widehat{B}\mathbf{u} + \dot{J}\dot{\mathbf{q}} \end{aligned} \tag{15}$$

The state vector is taken as $\mathbf{x} = \text{col}\{\dot{\mathbf{q}}, \mathbf{q}\}$ and the output is defined to be

$$\mathbf{y} = \ddot{\boldsymbol{\rho}} + \lambda\dot{\boldsymbol{\rho}} \quad \lambda > 0 \tag{16}$$

The system defined by Eqs. (12)–(16) can be identified with $\mathcal{G}$ of section 2 and written in the state form in (1) by defining

$$\mathbf{a}(\mathbf{x}) = \mathbf{A}(\mathbf{x})\mathbf{x} \quad \mathbf{c}(\mathbf{x}) = \mathbf{C}(\mathbf{x})\mathbf{x} \tag{17}$$

where

$$\begin{aligned} \mathbf{A} &= \begin{bmatrix} -M^{-1}(\widehat{D} + \widehat{C}) & -M^{-1}K \\ \mathbf{1} & \mathbf{O} \end{bmatrix} \\ \mathbf{C} &= \begin{bmatrix} -JM^{-1}(\widehat{D} + \widehat{C}) + \dot{J} + \lambda J & -JM^{-1}K \end{bmatrix} \\ \mathbf{d} &= JM^{-1}\widehat{B} \quad \mathbf{b} = \begin{bmatrix} M^{-1}\widehat{B} \\ \mathbf{O} \end{bmatrix} \end{aligned} \tag{18}$$

The underlying theory presented in section 2 requires that the system be controllable, observable, and asymptotically stable. The latter two do not apply to the joint coordinates $\boldsymbol{\theta}$, so they are removed from the state vector and in the sequel $\mathbf{x} = \text{col}\{\dot{\boldsymbol{\theta}}, \dot{\mathbf{q}}_e, \mathbf{q}_e\}$. However, the configuration dependence on $\boldsymbol{\theta}$ is maintained in M, J, $\widehat{C}$, and $\dot{J}$ with $\dot{\boldsymbol{\theta}} = [\mathbf{1} \; \mathbf{O} \; \mathbf{O}]^{\mathrm{T}}\mathbf{x}$ taken as a side condition. The reduced system then satisfies the required conditions.

The construction of the inverse of the outer factor in (6) requires the solution of the Hamilton–Jacobi equation in (10). An exact solution is not forthcoming but an approximation is possible using the so-called state-dependent Riccati equation.[15] Here, we approximate the solution of (10) by

$$P(\mathbf{x}) = \frac{1}{2}\mathbf{x}^{\mathrm{T}}\mathbf{P}(\mathbf{x})\mathbf{x} \quad P_{\mathbf{x}} \doteq \mathbf{x}^{\mathrm{T}}\mathbf{P}(\mathbf{x}) \tag{19}$$

which when used in conjunction with the linear-like factorizations in (17) yields the state-dependent Riccati equation (SDRE)

$$\begin{aligned} &\mathbf{P}(\mathbf{x})[\mathbf{A}(\mathbf{x}) - \mathbf{b}(\mathbf{x})\mathbf{d}^{-1}(\mathbf{x})\mathbf{C}(\mathbf{x})] \\ &\quad + [\mathbf{A}(\mathbf{x}) - \mathbf{b}(\mathbf{x})\mathbf{d}^{-1}(\mathbf{x})\mathbf{C}(\mathbf{x})]^{\mathrm{T}}\mathbf{P}(\mathbf{x}) \\ &\quad - \mathbf{P}(\mathbf{x})\mathbf{b}(\mathbf{x})[\mathbf{d}^{\mathrm{T}}(\mathbf{x})\mathbf{d}(\mathbf{x})]^{-1}\mathbf{b}(\mathbf{x})^{\mathrm{T}}\mathbf{P}(\mathbf{x}) = \mathbf{O} \end{aligned} \tag{20}$$

Given the state vector, the system matrices are evaluated and treated as constants so that the SDRE is treated like an algebraic Riccati equation. The required solution is that which stabilizes (11) in the same approximation, i.e., renders the system

$$\dot{\mathbf{x}} = [\mathbf{A} - \mathbf{b}\mathbf{d}^{-1}\mathbf{c} - \mathbf{b}(\mathbf{d}^{\mathrm{T}}\mathbf{d})^{-1}\mathbf{b}^{\mathrm{T}}\mathbf{P}]\mathbf{x}$$

asymptotically stable.

The static approximation to the inverse of the inner factor is determined by using (11) in conjunction with the definitions in (17) as well as $\bar{\mathbf{c}}(\mathbf{x}) = \mathbf{c}(\mathbf{x}) + \mathbf{d}^{-1}(\mathbf{x})\mathbf{b}^{\mathrm{T}}(\mathbf{x})\mathbf{P}(\mathbf{x})\mathbf{x}$, leading to

$$\begin{aligned}\bar{\mathbf{y}}_d &= \mathbf{y}_d - \mathbf{d}^{-\mathrm{T}}\mathbf{b}^{\mathrm{T}}\mathbf{P}[\mathbf{A} - \mathbf{b}\mathbf{d}^{-1}\mathbf{C}]^{-1}\mathbf{b}\mathbf{d}^{-1}\mathbf{y}_d \\ &= [\mathbf{1} - \mathbf{d}^{-\mathrm{T}}\mathbf{b}^{\mathrm{T}}\mathbf{P}(\mathbf{A} - \mathbf{b}\mathbf{d}^{-1}\mathbf{C})^{-1}\mathbf{b}\mathbf{d}^{-1}]\mathbf{y}_d\end{aligned} \tag{21}$$

which behaves like a static (orthogonal) transformation.

Assuming the desired trajectory for the endpoint, $\boldsymbol{\rho}_d(t)$, is known, the algorithm for determining the feedforward torques, reference trajectories for the joint angles, and feedback torques at time $t = t_k$ proceeds as follows:

Step 1. At time t_k we have the state vector $\mathbf{x}_k = \mathbf{x}(t_k)$ of $\mathscr{R}^{-1}$ as well as the joint angles $\boldsymbol{\theta}_k = \boldsymbol{\theta}(t_k)$. In particular, using the joint angles $\boldsymbol{\theta}_k$ and their rates $\dot{\boldsymbol{\theta}}_k$, form $\boldsymbol{M}$, $\boldsymbol{J}$, $\widehat{\boldsymbol{C}}$, and $\dot{\boldsymbol{J}}$. These are then used to assemble the state-dependent state matrices $(\mathbf{A}, \mathbf{b}, \mathbf{C}, \mathbf{d})$ in (18).

Step 2. Solve the SDRE in (20).

Step 3. Form $\bar{\mathbf{c}}(\mathbf{x}_k)$ according to

$$\bar{\mathbf{c}}(\mathbf{x}_k) = [\mathbf{C} + \mathbf{d}^{-1}\mathbf{b}^{\mathrm{T}}\mathbf{P}]\mathbf{x}_k$$

Step 4. Using $\mathbf{y}_d(t_k) = \ddot{\boldsymbol{\rho}}_d(t_k) + \lambda\dot{\boldsymbol{\rho}}_d(t_k)$ as the input, calculate the output $\bar{\mathbf{y}}_d$ of Θ_{ss}^{-1} using (21). Determine the feedforward torque according to the output of $\mathscr{R}^{-1}$ in (6): $\bar{\mathbf{u}}_d(t_k) = \mathbf{d}^{-1}[\bar{\mathbf{y}}_d(t_k) - \bar{\mathbf{c}}(\mathbf{x}_k)]$. From $\mathbf{x}_k$, extract the desired trajectory for $\dot{\boldsymbol{\theta}}(t_k)$.

Step 5. The total applied torque for the manipulator is given by $\mathbf{u}(t_k) = \bar{\mathbf{u}}_d(t_k) - \mathscr{H}[\bar{\boldsymbol{\theta}}(t_k) - \boldsymbol{\theta}_d(t_k)]$, where $\mathscr{H}$ denotes the feedback operator that is used, $\boldsymbol{\theta}_d(t_k) = \boldsymbol{\theta}(t_k)$, and $\bar{\boldsymbol{\theta}}$ is the actual measured joint motion.

Step 6. Determine $\dot{\mathbf{x}}(t_k) = \mathbf{a}(\mathbf{x}_k) + \mathbf{b}(\mathbf{x}_k)\bar{\mathbf{u}}_k$ which corresponds to (6) and use this to estimate $\mathbf{x}(t_{k+1})$. Use $\dot{\boldsymbol{\theta}}(t_k) = [\mathbf{1}\ \mathbf{O}\ \mathbf{O}]^{\mathrm{T}}\mathbf{x}(t_k)$ to estimate $\boldsymbol{\theta}(t_{k+1})$.

It is essential in constructing the inner–outer factorization that the matrix $\mathbf{d}$ defined in (18) remains invertible. Numerical experience has indicated that it may become close to singular. We have circumvented this problem by performing a singular value decomposition at each time step and latching any singular values satisfying $\sigma < 0.05$ at a value of $\sigma = 0.05$ followed by reconstruction of $\mathbf{d}$.

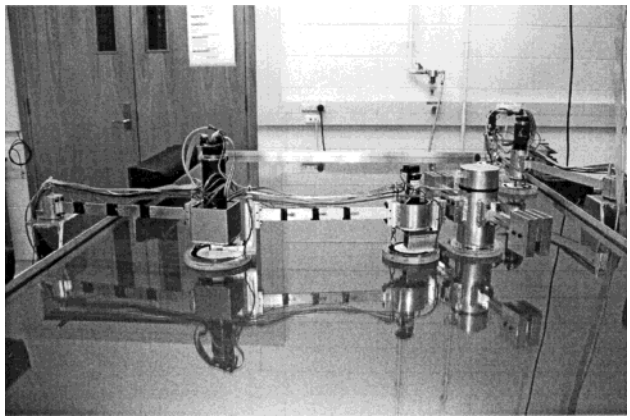

Figure 2. The experimental robot arm.

4. FEEDFORWARD AND FEEDBACK DESIGN

The performance of the above scheme was tested experimentally using the three-axis planar manipulator shown in Figure 2. The first two links were structurally flexible while the third was a rigid link to the payload. The properties are summarized in Table I. The actual payload that was used is somewhat smaller than that shown in Figure 2. Current control through DC motors and low backlash gearboxes provided the torque for each axis. Sensing involved quadrature encoders on the joints, three strain gauges distributed along each flexible link, and a CCD camera to detect the position and orientation of the payload. For control purposes, only the joint angles were used as feedback.

The feedback controller was implemented using a series of decoupled second-order lead compensators wrapped around each joint. Good damping of the closed-loop poles was achieved, even with the change in dynamic properties as the configuration of the arm varied. If the output of the arm is taken to be joint rate and an integrator is included in the controller, then the controller is strictly positive real (SPR) and the plant is PR. Hence, we have exploited the passive map from joint torques to joint rates and implemented an SPR feedback controller which provides robust stability.

Table I. Link properties.

Property	Link 1	Link 2	Link 3
EI ($\mathrm{N\,m^2}$)	39	39	Rigid
Arm Mass (kg)	0.19	0.16	0
Hub Mass (kg)	2.53	2.10	0.97
Tip Mass (kg)	2.23	0.94	2.37
Length (mm)	500	500	170

Two different methods of generating the feedforward were used: (i) use of the "full" nonlinear dynamics as outlined in section 3; (ii) the use of modal transformation of Eq. (12) which preserved the nonlinear rigid dynamics but superimposed a constant frequency/constant mode shape description for the unconstrained vibration modes. Both of these schemes involved solving the SDRE at each time step of the integration. Method (i), which was expected to give the best results, yielded a set of equations that were difficult to integrate. Only the results for method (i) will be presented in the next section since those obtained using method (ii) were very similar.

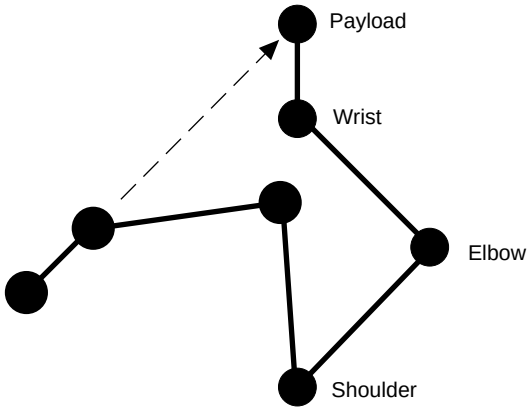

Figure 4. Maneuver 2 arm position.

5. EXPERIMENTAL RESULTS

Results will be presented for two maneuvers. The first is a movement of 670 mm in the negative y-direction (Figure 3) and the second is a 940 mm movement involving all three tip coordinates (Figure 4). The start and finish points are given in Tables II and III. To give a smooth acceleration profile, the desired path was generated using a fifth-order polynomial fitted to the start and finish points. The time for the maneuver in both cases was 1.5 s.

The integration of the state equations in (6) yielded prescribed tip trajectories which tended to drift slightly from the desired path as time progressed. Part of this stems from the causal approximation while some of it is numerical in origin. Since $\mathscr{R}$ preserves the steady-state properties of $\mathscr{G}$, the final endpoint should be the same as the prescribed trajectory. This property hinges on the solution of the Hamilton–Jacobi equation. Since this has been approximated by the SDRE, this property does not hold exactly. This was surmounted by reformulating the prescribed trajectory $\mathbf{y}_d$ near to the end of the maneuver using the current state of the arm and the desired target configuration. The identification of the states of $\mathscr{R}^{-1}$ with the desired ones of $\mathscr{G}$ continues to hold given the form of $\mathscr{R}^{-1}$ in Eq. (6) which continues to mimic Eq. (1) with the appropriate $\mathbf{u} = \mathbf{u}_d$.

The use of two different feedforward signals (with identical feedback controller) will be compared: the use of the full equations to obtain the causal feedforward (method (i) above) and rigid inverse dynamics using the rigid inverse kinematics to obtain the reference trajectories. The tip motion of

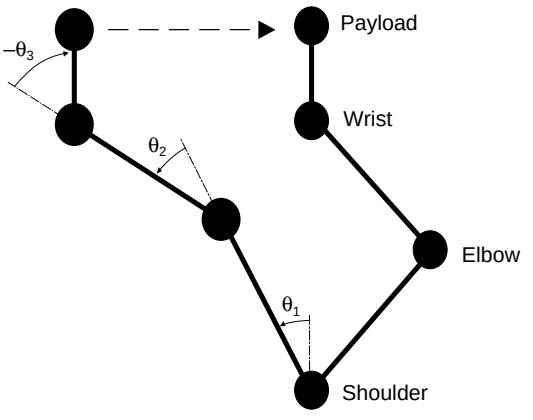

Figure 3. Maneuver 1 arm position.

Table II. Maneuver 1 endpoints and tracking errors.

	Path		Maximum error		
Tip position	Start	Stop	Rigid	Full eqs.	Fixed modes
$\mathbf{x}\,(m)$	0.94	0.94	0.048	0.021	0.022
$\mathbf{y}\,(m)$	0.67	0	0.162	0.064	0.066
ϕ (rad)	0	0	0.259	0.095	0.100

Table III. Maneuver 2 endpoints and tracking errors.

	Path		Maximum error		
Tip position	Start	Stop	Rigid	Full eqs.	Fixed modes
$\mathbf{x}\,(m)$	0.30	0.94	0.057	0.075	0.067
$\mathbf{y}\,(m)$	0.67	0	0.127	0.060	0.047
ϕ (rad)	2.36	0	0.227	0.092	0.098

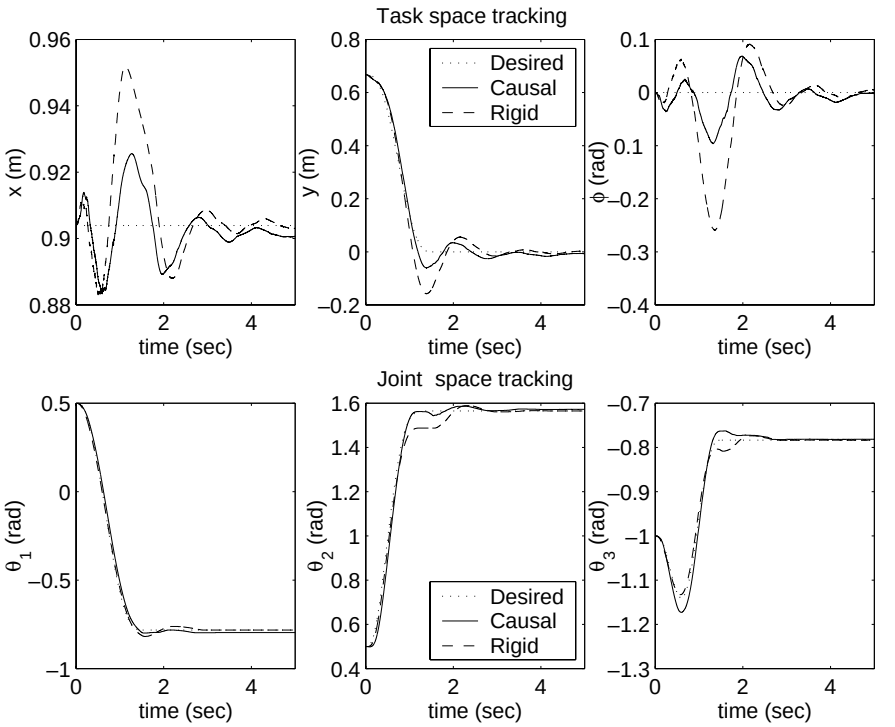

Figure 5. Maneuver 1 tip position and joint angles.

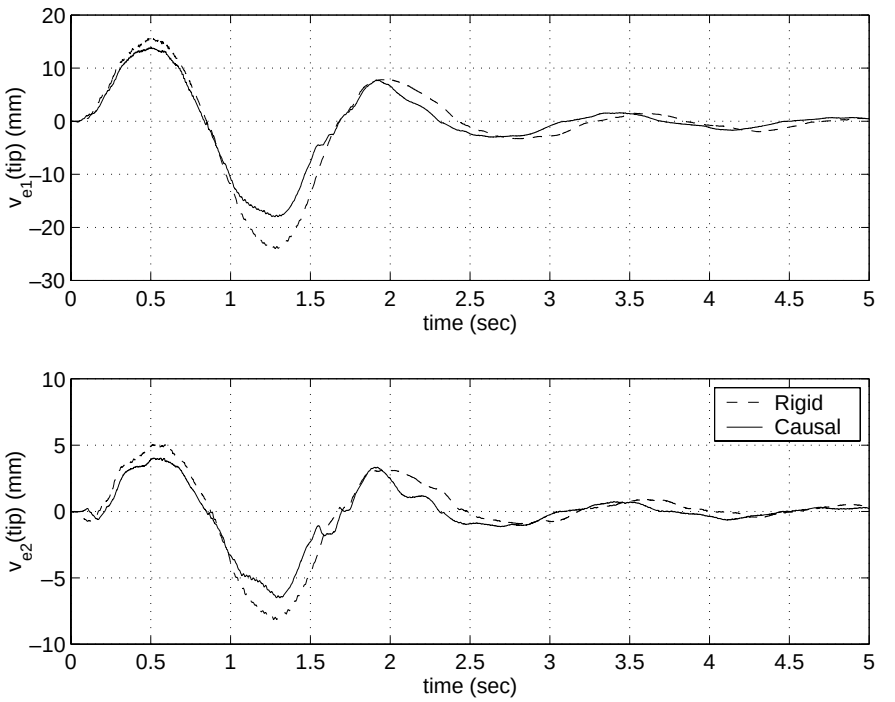

Figure 6. Maneuver 1 link deflections.

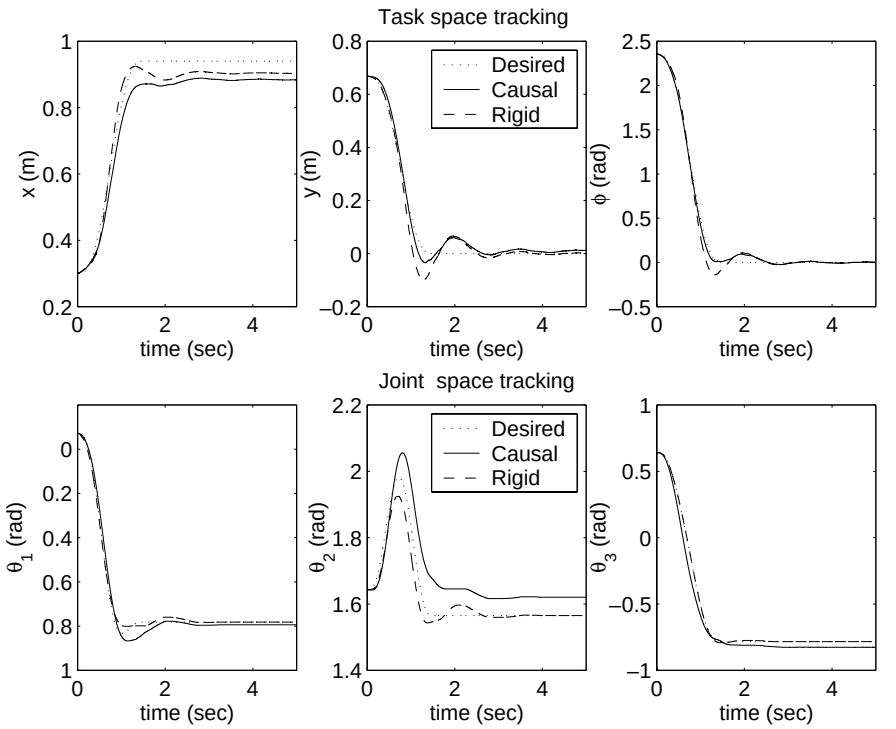

Figure 7. Maneuver 2 tip position and joint angles.

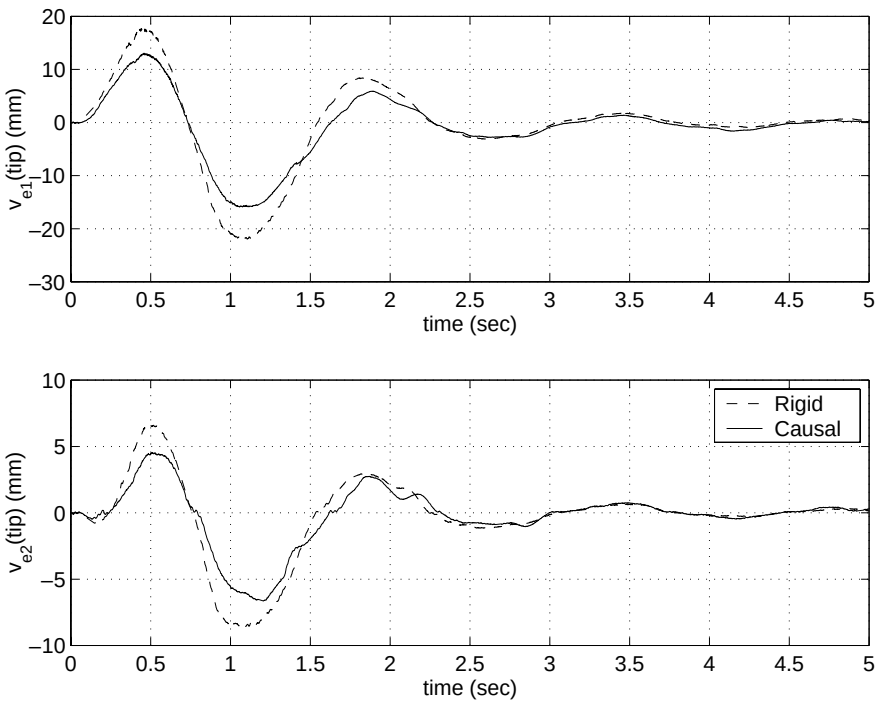

Figure 8. Maneuver 2 link deflections.

the manipulator in each case is shown in Figures 5 and 7. The maximum error with respect to the desired path is shown in Tables II and III. A value of $\lambda = 30$ s was used in Eq. (16).

As can be seen from the tables, the feedforward based on the full equations and that based on the fixed modes gave very similar results, with maximum errors of about 40% of the error for the rigid feedforward. Using simulation instead of the real manipulator produced a very similar tip trajectory. Because the simulation and the feedforward were based on the same model, the error is assumed to come from the approximation that forces the feedforward to be causal rather than being produced by modeling errors. This shows that the causal approximation to the inverse does not give perfect tip tracking, but is a significant improvement over the rigid inverse dynamics. From Table III and Figure 7, we see that the static approximation to the inverse of the inner factor leads to improvements in the y- and ϕ-tracking at the expense of the x-tracking behavior.

In Figures 6 and 8, the tip deflections of links 1 and 2, v_{e1} and v_{e2}, respectively, are shown for each maneuver. Both sets of curves show that the causal feedforward leads to reduced elastic deflections for the links relative to the rigid feedforward case.

6. CONCLUSIONS

A control scheme for tip-trajectory tracking by structurally flexible manipulators has been presented which avoids the noncausal nature of the inverse dynamics map. Nonlinear inner–outer factorizations of the forward dynamics map have been used to generate an approximate causal inverse which provides a feedforward torque and a means of generating reference trajectories for the joint angles. This represents a simpler feedback design problem given the collocated and passive nature of the torque to joint rate map.

The experimental results showed that reasonably good tracking of the prescribed end-effector trajectories was possible using this approach. The main contribution of this work is a framework for approximating the inverse dynamics of flexible arms under the restriction of causality.

REFERENCES

1. A. DeLuca and B. Siciliano, Inversion-based nonlinear control of robot arms with flexible links, J Guidance Contr Dynamics 16 (1993), 1169–1176.
2. E. Bayo, P. Papadopoulos, J. Stubbe, and M. Serna, Inverse dynamics and kinematics of multi-link elastic robots: an iterative frequency domain approach, Int J Robot Res 8 (1989), 49–62.
3. S. Devasia, D. Chen, and B. Paden, Nonlinear inversion-based output tracking, IEEE Trans Automat Contr 41 (1996), 930–942.
4. H. Zhao and D. Chen, Tip trajectory tracking for multilink flexible manipulators using stable inversion, J Guidance Contr Dynamics 21 (1998), 314–320.
5. D.-S. Kwon and W.J. Book, A time-domain inverse dynamic tracking control of a single-link flexible manipulator, J Dynamic Syst Meas Contr 116 (1994), 193–200.
6. B. Paden, D. Chen, R. Ledesma, and E. Bayo, Exponentially stable tracking control for multijoint flexible-link manipulators, J Dynamic Syst Meas Contr 115 (1993), 53–59.
7. D. Wang and M. Vidyasagar, Transfer functions for a single flexible link, Int J Robot Res 10 (1992), 540–549.
8. C.J. Damaren, Passivity analysis for flexible multilink space manipulators, J Guidance Contr Dynamics 18 (1995), 272–279.
9. M. Moallem, R.V. Patel, and K. Khorasani, An inverse dynamics control strategy for tip position tracking of flexible multi-link manipulators, J Robot Syst 14 (1997), 649–658.
10. E. Gross and M. Tomizuka, Experimental flexible beam tip tracking control with a truncated series approximation to uncancelable inverse dynamics, IEEE Trans Contr Syst Technol 4 (1994), 382–391.
11. D.E. Torfs, R. Vuerinckx, J. Swevers, and J. Schoukens, Comparison of two feedforward design methods aiming at accurate trajectory tracking of the end point of a flexible robot arm, IEEE Trans Contr Syst Technol 6 (1998), 2–14.
12. U. Shaked, The all-pass property of optimal open-loop tracking systems, IEEE Trans Automat Contr 29 (1984), 465–467.
13. J.A. Ball and A.J. van der Schaft, J-inner–outer factorization, J-spectral factorization, and robust control for nonlinear systems, IEEE Trans Automat Contr 41 (1996), 379–392.
14. K. Zhou, J.C. Doyle, and K. Glover, Robust and Optimal Control, Prentice-Hall, New Jersey, 1996.
15. K.D. Hammett, C.D. Hall, and D.B. Ridgely, Controllability issues in nonlinear state-dependent riccati equation control, J Guidance Contr Dynamics 21 (1998), 767–773.